Microelectronic Engineering 5 (1986) 203–216
North-Holland

QUANTUM TRANSPORT IN MICROSTRUCTURES*

Daniel E. PROBER

Section of Applied Physics, Yale University, P.O. Box 2157
New Haven, CT 06520 USA

Advanced microfabrication techniques allow production of experimental systems as narrow as 20 nm for study of electron transport at low temperatures, ~1K. Fine wires in metals, Si-MOS inversion layers, and GaAs modulation-doped heterostructure layers have been studied. Metal rings of diameter ~1 μm have also been studied. New electron interference effects have been discovered in these systems, due to electron partial waves which scatter elastically from impurities. The length scale over which these interference effects occur is the phase coherence length, ℓ_ϕ, of order 1 μm or greater at 1K. In this paper the physical mechanisms and manifestations of these electron interference effects are reviewed. The microfabrication methods used to produce these ultrasmall structures are also reviewed. Other quantum transport issues, including inelastic scattering mechanisms, detection of single trap states, and wavefunction spatial quantization, are also discussed.

Rapid advances in microfabrication technology have allowed steady increases in circuit complexity and reductions in minimum feature size. Advanced ICs have minimum linewidths of order 1 μm. The trend toward smaller features and (possibly) toward reduced operating power and temperatures strongly commends full investigation of the limits on device scaling and the opportunities which may be found in yet smaller devices.

The tools of the microcircuit industry now provide scientists with the means to fabricate sub-0.1-micron structures for studies of transport physics. Many of the transport issues presently being studied are fundamental in nature, and occur in the liquid-helium temperature range ($T \lesssim 4.2K$). Nevertheless, even skeptics will have to admit that such transport phenomena may be of practical importance in future decades.

The purpose of this paper is to review recent developments on quantum effects on electron transport in sub-100-nm structures. The intent is to be tutorial rather than all encompassing. It is our intent to convey the main physical ideas, with a minimum of formalism. We develop a unified physical picture for electron localization effects, conductance fluctuations, and Aharonov-Bohm oscillations in rings. Readers are referred to numerous excellent reviews for more formal treatments.[1-10]

1. QUANTUM TRANSPORT REGIME

As semiconductor device sizes approach 0.1 μm, various quantum effects become evident. In a metal or semiconductor with no scattering, the electron wave function can be described by

$$\psi = |\psi| e^{i\phi} = |\psi| e^{i[\vec{k}\cdot\vec{r}-(Et/\hbar)]} \quad . \tag{1}$$

At low temperatures, the time between inelastic (energy exchange) scattering events is relatively long ($\Delta t \gtrsim 10^{-8}$ s), so the electron energy ($\propto$ frequency)

*Research programs at Yale University supported by NSF grants DMR-8505539, ECS-8509135, and ECS-8604350. Additional facilities support for the research described herein provided by IBM and Shipley Co.

Table I Experimental Systems for 2D and 1D Transport Studies. All systems are degenerate electron gases: $k_BT \ll E_F$ for typical experimental conditions. Also, the electron density is essentially temperature independent, so that the resistance is only weakly dependent on T. For the Si MOSFETs and GaAs layers, the electron density is typically low enough that the electron is in its lowest quantized state in the triangular potential well perpendicular to the surface, [10] so that the electron system is strictly 2D. Mobility $\mu = e\tau/m$.

	Metal	MOSFET	GaAs
Conductor thickness, d	~10-40 nm	~3 nm	~8 nm
Electron density	fixed ~10^{22} cm^{-3}	controllable n_s~10^{12} cm^{-2} $\propto(V_G-V_T)$	~fixed; can change with light n_s~ 5 x 10^{11} cm^{-2}
Fermi energy	fixed ~10 eV	controllable ~10-50 meV, $\propto(V_G-V_T)$	~fixed
Examples	Au,Ag,Al	<100> Si with 20 nm oxide	GaAs-Ga$_{.7}$Al$_{.3}$As
μ_{max}(cm^2/V-sec)	50	20,000	~2x10^6
Elastic mean-free path, ℓ	~10 nm	~10-100 nm	~10 μm
Smallest structure fabricated & studied	15 nm	~20 nm	~100 nm

is constant for relatively long times and distances (~1 μm). As a result, electron partial waves emanating from an impurity scattering site (elastic scattering) can interfere with each other over "macroscopic" distances (~1 μm). These interference effects are the main subject of this paper.

In what types of samples are interference effects seen? In 3 main systems: 1. clean metal films and wires, where the elastic (energy conserving) scattering length ℓ is ~1-10 nm; 2. Si MOSFET inversion layers, both wide (2-dimensional) strips and narrow (1D) strips; and 3. GaAs modulation-doped heterostructures, both wide (2D) and narrow (1D). The main features of each system are outlined in Table I.

The length scale determining whether a system is 1-, 2- or 3-dimensional for the quantum interference effects is the electron phase-coherence length, ℓ_ϕ. Since the phase-coherence time τ_ϕ (~10^{-8}s), is much longer than the elastic scattering time (τ~10^{-14}s in metals), the electron motion is **diffusive** between phase-breaking events. (This diffusive motion, shown in Fig. 1, looks like a random walk with steps of length $\ell = v_F\tau$, with v_F the Fermi velocity.) Thus,

$$\ell_\phi = (D\tau_\phi)^{1/2} \qquad (2)$$

with $D = v_F\ell/2$, the 2D diffusion constant. The Fermi energy is $E_F = mv_F^2/2 = \hbar^2k_F^2/2m$. A metal wire which is **one**-dimensional for the quantum-interference effects is illustrated in Fig. 1.

Inelastic collisions contribute to phase breaking. When E is changed by a large amount the frequency = $E/\hbar$ also shifts, and interference with a second wave having the original frequency is no longer possible. Phase "memory" is thus destroyed. The phase-breaking rate τ_ϕ^{-1} has contributions from electron-phonon scattering and from electron-electron scattering:

$$\tau_\phi^{-1} = \tau_{e-ph}^{-1} + \tau_{e-e}^{-1} \quad . \tag{3}$$

For wide films, the electron-electron rate is 2D, [4] while for narrow wires the e-e rate is 1D and depends explicitly on the wire width W.[11] This is discussed in detail in Sec. 4.1. At 1K, a typical rate is $\tau_\phi^{-1} \sim 10^8 s^{-1}$. Thus, for $D = 1\ cm^2/s$, ℓ_ϕ is indeed ~1 µm.

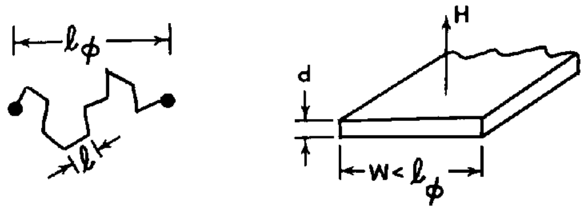

Fig. 1 Diagram of microscopic electron motion and 1D wire.

2. FABRICATION

The discussion above indicates that in order to produce 1-dimensional wires, the linewidth must be less than $\ell_\phi \sim 1$ µm. However, the linewidth required is typically much smaller than 1 µm. This is for 2 reasons: First, to study the effects of one-dimensional electron-electron scattering on inelastic scattering, a wire must be narrower than the "thermal" diffusion length $\ell_T = (\hbar D/kT)^{1/2} \sim 0.2$ µm in metal wires. Second, for quantum-interference effects in a ring structure, the path length around the ring must be of order ℓ_ϕ. The linewidth must be significantly less than the diameter, to ensure that the magnetic flux (field x area) within the area of the metal wires is much less than that enclosed by the ring. With this condition met, ring interference effects are clearly visible. [12] Thus, a linewith requirement of 0.02 - 0.1 µm arises for fabrication of wires and rings.

We discuss here the fabrication approaches developed for metal structures. For Si MOSFETs and heterostructures, one encounters even greater challenges in producing structures this small, due to the complex and interacting materials issues. We refer the reader to Ref. 8 for a fuller discussion.

Si MOS channels as narrow as 20 nm have been studied at ATT-Bell Labs [13]. The basic approach is to pattern the gate electrode by e-beam lithography and lift-off, and then to etch that pattern by reactive-ion etching into the SiO_2 and underlying Si. An alternate approach, used at Yale [14] and MIT [15,16] is to use a thin oxide, so that the width of the inversion layer accurately replicates the gate pattern (dual-gate in Ref. 16). Inversion layer widths ~50 nm have been achieved in the dual-gate approach, using x-ray patterning for the lower, grating gate. Researchers at Cambridge [17] and IBM [18] have used a split gate configuration to produce narrow Si inversion layer wires. The inversion layer is pinched down from each side. GaAs-heterostructure wires have been produced in the split-gate configuration [19] and using simpler substrate etching methods. [20]

Fabrication of metal wires can be accomplished with various step-edge techniques [7,21, 21a], x-ray replication [4a], or e-beam lithography. The

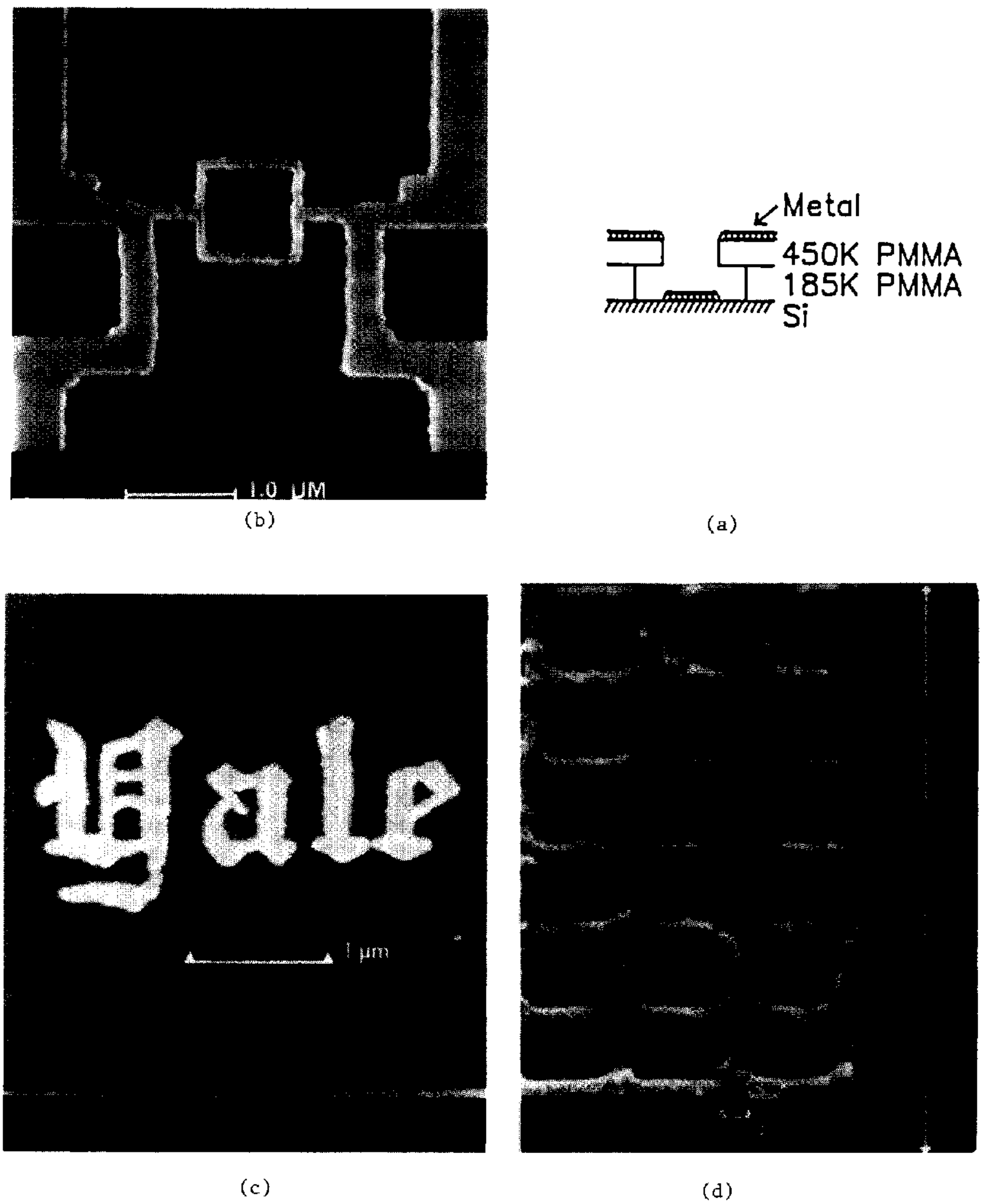

Fig. 2 a. Schematic of PMMA bilayer resist with evaporated metal, showing undercut profile; prior to lift-off. b. Ring pattern, 1-µm square metal ring; produced by e-beam patterning of single-layer resist and lift-off. c. Metal pattern, Au on oxidized Si; d. Dense high-resolution metal pattern produced by liftoff; repeat distance is 150 nm; mimimum linewidth ~35 nm. Good integrity of the resist liftoff mask, 110 nm squares of undercut PMMA, can be inferred.

narrowest wires studied to date, W = 15 nm, have used step-edge techniques! [21a] Nevertheless, for metal patterns e-beam lithography is preferred - for its material and pattern flexibility and for its ability to produce complex patterns, such as rings and arrays of rings, in a 4-terminal configuration (Fig. 2b). A potential disadvantage of e-beam patterning is that it can damage underlying layers, such as the MOS oxide. However, for metal patterns this is not a problem.

The e-beam patterning method developed at Yale uses a standard ISI SS-60 SEM with the beam-blanker accessory. A raster scan is used. For moderate size structures (linewidth $\geq$ 100 nm), a single layer of PMMA 0.3 μm thick is used. For structures with the smallest linewidths, a bilayer resist is employed to ensure an undercut profile. This bilayer resist consists of 60 nm PMMA (molecular weight 450K) on top of 60 nm PMMA (molecular weight 185K). The lower molecular weight layer develops faster. For the single layer and the bilayer, the developer is MIBK:IPA, 1:3. The bilayer is shown in Fig. 2a. Metal liftoff is accomplished by spraying with acetone. [9] The processing is described in detail in a separate publication. [22] The narrowest metal line produced is 30 nm wide. Examples of metal patterns produced are shown in Fig. 2b-2d. A higher resolution exposure tool should be able to achieve much narrower linewidths. [9]

A common problem with bilayer resists is the tendency of the lower layer to intermix with the upper layer when the latter is spun on. We avoid this by using a relatively weak solvent, xylene, [9] as the casting solvent for the upper layer. Intermixing appears to be negligible.

E-beam patterning is too slow to expose large areas, particularly with an SEM. We therefore expose the large area patterns in the PMMA with deep-UV ($\lambda \sim 220$ nm) and develop this pattern prior to e-beam exposure of the fine features. The e-beam exposure can typically be aligned rather easily to this dUV-exposed pattern, if oxidized Si substrates are used.

3. QUANTUM-INTERFERENCE EXPERIMENTS

There are two basic geometries in which the quantum-interference effects alluded to above can be studied: narrow wires (singly-connected geometry) and rings. Two- and three-dimensional samples show interference effects, [1-3] as do wires. However, the effects become stronger, and often are conceptually simpler, in the 1D geometry. In general, the lower the system dimensionality, the larger the effect.

As an illustration, consider the case of a short wire with various impurity scattering sites but without inelastic scattering. If the input (from the left) is an electron plane wave, the output (on the right) is a distorted wave which reflects the exact scattering properties of each impurity. The transmission through this section of wire thus depends on the microscopic impurity configuration. For two samples with different microscopic impurity distributions, the output waves and the reflected waves may be quite different. The current flow may thus be quite different for these two samples. The complexity of calculating the transmission properties can be reduced if one instead computes the interference of electrons along the various paths defined by the impurity distribution.

3.1. One-Dimensional Localization

In Fig. 3a, we consider an input wave from the left which splits into **two** partial waves which travel on identical paths, in opposite directions, back to the origin. Since the two paths are identical, the two waves arrive back at the origin **in phase** with each other. (This assumes, of course, that ℓ_ϕ is much greater than the path length.) The two returning waves interfere **constructively** at the origin since they have traversed the same path and the energies are unchanged. Thus, the probability of returning to the origin (a back-echo) is large. All electron paths which are time-reversed pairs contribute to the back-echo.

If one of the two waves in Fig. 3a had changed its energy (i.e., **lost** its phase memory along the path), the two waves could not have a time independent interference back at the origin. The net back-echo would thus be negligible. This is the high-temperature case, where phonon scattering is rapid.

The back-echo increases the wire resistance. The electron has a larger chance of returning to the input, and thus a reduced chance of transmitting through the wire. The electron gets "stuck"; this is known as localization. The prediction for the decrease in conductance $G = R^{-1}$ due to localization is

$$\delta G = 2(e^2/h)\,\frac{\ell_\phi}{L}\,, \qquad (4)$$

with e the electron charge, h Planck's constant and L the wire length. This formula applies for $L > \ell_\phi$. Thouless was the first to make such a prediction. His starting model [23] considered quantum diffusion of wave packets, which is more intuitive for the very-low-temperature regime where the electron is strongly localized. (Eq. 4 is applicable when the electron is weakly localized, $\delta G/G \ll 1$). However, the two pictures are, in fact, equivalent.

Inelastic scattering becomes less frequent as the temperature is reduced. Thus, both ℓ_ϕ and the quantum correction, Eq. 4, increase as T decreases. This introduces a temperature dependence to the resistance. Spin-orbit and magnetic scattering modify the quantitative predictions, as do superconducting fluctuations. [4,11,15] Nevertheless, the physical picture of interference giving rise to a back-echo is still correct.

It turns out that the magnetoresistance is a more sensitive quantity than R(T) for probing localization effects. This is because other quantum corrections (e.g., electron interaction effects) contribute to the temperature dependence of R at low temperatures. These other corrections do not contribute to the low-field magnetoresistance. The effect of a magnetic field on the localization correction is more easily explained for the ring geometry, and is discussed later.

Localization effects have now been extensively studied in 2D and 1D systems of metal films, MOSFETs, and heterostructures. The physical picture and quantitative predictions for the electron back-echo are now very well established. Analogous photon back-echoes [24] have more recently been predicted and studied in optical scattering from "smoke" samples. Coherent back-echoes seem to be a ubiquitous, though previously unappreciated, phenomenon for waves in random media.

3.2. Conductance Fluctuations

A second type of quantum interference effect is seen in wires when one considers **non-equivalent** interference paths (Fig. 3b). This effect is strongest in short, narrow wires. For the paths shown in Fig. 3b, the 2 electron partial waves interfere at the output. A simple model for the intensity resulting from two interfering paths is

$$I = |\psi_1 + \psi_2|^2 = |\psi_1|^2 + |\psi_2|^2 + |\psi_1||\psi_2|\cos(\phi_1 - \phi_2) \qquad (5)$$
$$\sim 2|\psi|^2[1 + \cos(\phi_1 - \phi_2)]$$

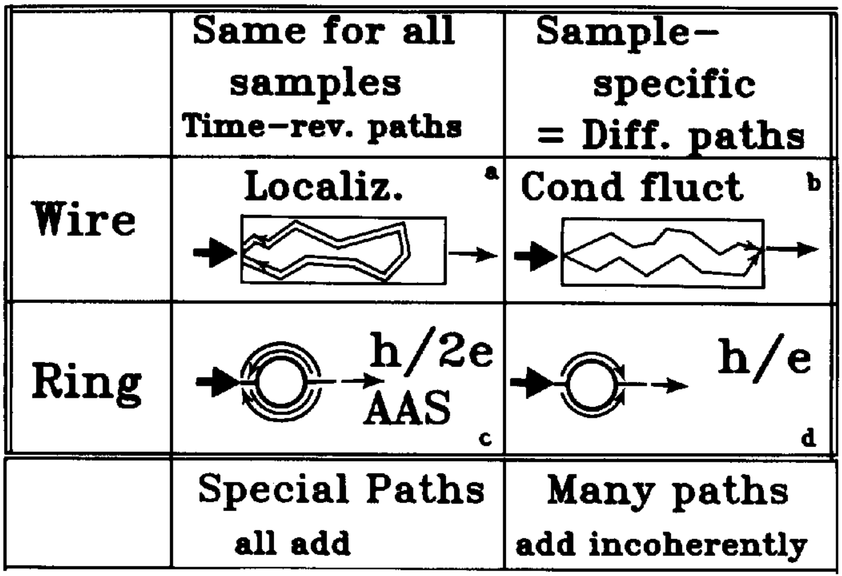

Fig. 3 Summary of quantum transport effects.

Whether the resulting intensity reflects constructive ($\phi_1-\phi_2 = 0$) or destructive interference depends on the difference between the phase increments along the 2 paths. The phase difference thus depends on the microscopic impurity location along each path. For small samples there are not so many different paths, so some amount of constructive (or destructive) interference will survive the averaging over all paths. The total sample conductance will then be larger (or smaller) than it would be if phase memory were lost in traversing the sample. (Loss of phase memory corresponds to setting the cosine term in Eq. 5 equal to zero.) To the extent that the interference term survives when averaging over all paths, the resistances of samples with microscopically different impurity locations will be different. This unexpected difference between macroscopically identical samples is referred to as conductance fluctuations. [25,26] The rms conductance variation for an ensemble of macroscopically identical, short wires is [25]

$$\delta G^{fluct} \sim 0.5\ e^2/h. \qquad (6)$$

The fact that this is a universal prediction, with a value given by fundamental physical constants, is most striking. Good evidence for this predic-

Table II - Factors affecting phase increment along an electron's path.

Energy E_F:	$\hbar^2k^2/2m = E_F$; phase increment, $\phi = \vec{k}\cdot\vec{r}$, changes with E_F
Temperature:	Thermal distribution of energies (k values) around E_F; a distribution of values for ϕ results at high temperatures.
Magnetic field:	$\Delta\phi = (e/\hbar)\int\vec{A}\cdot d\vec{\ell}$ along electron path; $\vec{A}$ = magnetic vector potential; $\vec{B}$ = curl $\vec{A}$

tion, and the dependence on sample length for $L > \ell_\phi$, has recently been presented. [18,27]

There are a number of ways one can change the phase increment along a specific path. These are listed in Table II. Changes in temperature and, for MOSFETs, $E_F(\propto V_g)$, are readily accomplished, and their effect on the conductance fluctuations is seen. The effect of magnetic fields is evident in metal films and MOS samples. [18,27,39]

3.3 Quantum-Interference in Rings: Theory

Consider the ring and the electron paths shown in Fig. 3c. Here the electron enters from the left, and splits into 2 partial waves which travel on **identical** but time-reversed paths back to the origin. Since the microscopic scattering paths are identical, in zero field ($A = 0$) the 2 electron waves return to the origin with the **same** phase increment. The 2 waves thus interfere constructively at the origin. This is equivalent to the electron backward echo discussed before. It occurs when the electron phase is preserved along the path length. If ℓ_ϕ were instead much less than the ring perimeter, the back-echo would **not** be seen. The quantum back-echo is seen in rings, wires and films. The result of the electron back-echo is again to **increase** the resistance, since the electron is more likely to return to the origin, rather than be transmitted through the ring.

What is the effect of a magnetic field? The magnetic field $\vec{B}$ arises from a magnetic vector potential $\vec{A}$: $\vec{B} = \text{curl } \vec{A}$. The extra electron phase increment due to $\vec{A}$ in going clockwise around the ring is, for each electron, $\phi_{cw} = e/\hbar \oint \vec{A}.d\vec{\ell}$, with e the electron charge and $\hbar$ = Planck's constant/2π. Thus, the phase **difference** between the 2 counterpropagating waves is

$$\Delta\phi = 2(e/\hbar) \oint \vec{A}\cdot d\vec{\ell} = 4\pi(\Phi/\Phi_o), \tag{7}$$

with Φ the enclosed magnetic flux = B x Area, and Φ_o the single-electron flux quantum, h/e. As a result of this phase difference, in a magnetic field the full back-echo is observed (resistance is increased) only when $\Delta\phi = 2\pi n$ with n an integer; this requires $\Phi = n\Phi_o/2 = nh/2e$. The back-echo is destroyed when $\Phi = (n + 1/2)\Phi_o/2$. The resistance should thus oscillate with a flux period of $h/2e = 2.07 \times 10^{-7}$ G-cm^2. For a 1 μm^2 ring, a period of 20.7 G is predicted.

Electron-interference effects periodic in the applied magnetic flux are known from quantum theory (for electrons in **vacuum**) as the Aharonov-Bohm effect. Prior to 1981, it had been believed (incorrectly) that the scattering in a typical metal film, with mean free path ℓ = 10 nm, would destroy such interference effects. For electrons in a thin-film metal ring or cylinder of diameter >> 10 nm, interference effects were first predicted in 1981, by Altshuler, Aronov, and Spivak (AAS) [28]. The requirement for observation is ℓ_ϕ ~ ring diameter. Because the two electron waves travel on **identical** paths back to the origin, (elastic) impurity scattering does not destroy this effect. The exact microscopic location of the impurities is **not** important for this effect, as was also true for the localization back-echo, Fig. 3a. Thus, all rings with the same **macroscopic** impurity content will have identical behavior, as long as the ring is small, with perimeter $<\ell_\phi$. Recent predictions [29] of the AAS effect show that the ring conductance for small rings at low temperature will oscillate as given by Eq. 8. Again, the behavior is universal. The flux repeat period is h/2**e**:

$$\delta G \sim -0.04(e^2/h) \cos (4\pi\Phi/\Phi_o) \quad . \tag{8}$$

The AAS prediction was initially greeted with much skepticism in the West. The experiments by Sharvin and Sharvin [30] which observed this effect in hollow Mg cylinders, 1 μm in diameter, also met with surprise. Both proved to be entirely correct.

A second type of ring interference effect is shown in Fig. 3d. Here the electron interference takes place at the output of the ring. The phase **difference** is no longer the same for all pairs of paths. The two paths are non-equivalent, so that the phase difference (Eq. 5) is random. Another pair of paths will have another phase difference. Thus, the intensity from all sets of paths may have net constructive or destructive contributions, depending on the **microscopic** impurity distribution. This is the same situation as for the conductance fluctuations, Fig. 3b. For the ring, the application of a magnetic field leads to conductance oscillations with a flux period of h/e, since the flux adds to all phase differences. The factor of 1e results because the magnetic flux is encircled once by the 2 electron waves. In the AAS effect, the magnetic flux is encircled twice, leading to the h/2e periodicity there.

The first prediction of resistance oscillations of period h/e were made in 1984 for an idealized ring; [31] predictions for a more realistic ring were presented subsequently [32]. Recent calculations [29] of this effect for small rings at low temperatures yield

$$\delta G \sim 0.4(e^2/h)\cos[(2\pi\Phi/\Phi_o) + \gamma_o] \quad . \tag{9}$$

Here γ_o is a phase factor specific to each ring. It reflects the **microscopic** impurity distribution.

We note that similar random-phase interference can also occur between two waves which propagate fully around the ring back to the origin on **non-equivalent** paths. The flux period is h/2e for this case. However, such non-equivalent paths are not the time-reversed pairs considered by Altshuler et al. The h/2e effect for non-equivalent paths may therefore be termed the non-AAS h/2e term. Its phase can be random, as in Eq. 9, and this non-AAS term is weaker than both the h/e and the AAS h/2e term. We therefore describe below all interference effects arising from non-equivalent paths as "h/e" interference.

If one were to measure h/e resistance oscillations in an array of such rings, each with its own γ_o, the normalized resistance oscillations would be smaller than for a single ring. The amplitude decreases as $\propto N^{-1/2}$, with N the number of rings in the array. This is because the γ_o's are random variables. The AAS effect, in contrast, has the same magnitude in an array as in a single ring, since $\gamma_o = 0$ for equivalent paths. The AAS effect is also different in that it is suppressed by moderate magnetic fields (>200 G), whereas the h/e oscillations persist to very large fields.

3.4. Quantum-Interference in Rings: Experiment

The first experiments on Aharonov-Bohm effects in metal film structures were by Sharvin and Sharvin,[30] who studied Mg films evaporated onto a 1-μm diameter fiber. Subsequent experiments by various groups on similar Li, Mg, and Al cylinders verified the AAS predictions in quantitative detail. Experiments have also been conducted on arrays of thin-film rings [33,35] in which qualitatively similar behavior is seen. The quantitative understanding of arrays is not yet complete [34]. In large arrays and in cylinders, only the AAS h/2e oscillations have been seen.

Even with the above results for cylinders and arrays, until 1984 numerous experiments on **single** rings failed to find either of the predicted interference effects. This was particularly puzzling, as a single ring is presumably the simplest case theoretically.

The first clear experimental observations of Aharonov-Bohm oscillations in single rings were made in 1985 by Webb et al. [36], who studied h/e and, later, also AAS h/2e oscillations in Ag rings [40], by Chandrasekhar et al. at Yale, who found both h/e and AAS h/2e oscillations in Ag rings, and h/2e oscillations in Al rings [37], and by Datta et al. [38] who studied rings formed by two heterostructure conducting layers. Earlier reports on rings by the IBM group [39] had shown some indications of h/e oscillations and conductance fluctuations, as a function of field. Data from the Yale experiments are shown below.

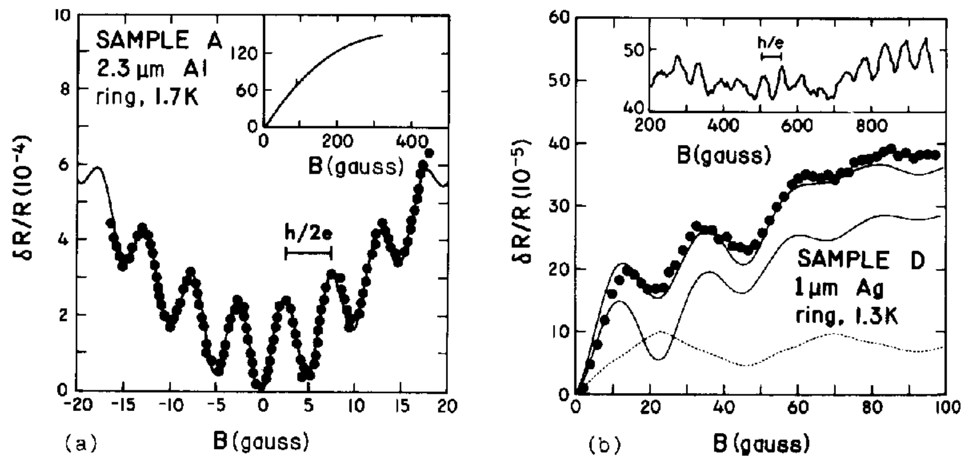

Fig.4 a. (left) Magnetoresistance of 2.3-μm diameter Al ring, linewidth 0.19 μm, 15 nm thick. Low-field AAS oscillations are clearly evident. Solid curve is theoretical fit, with ℓ_ϕ = 1.7 μm. b. Magnetoresistance of 1.0-μm diam. Ag ring. Heavy dots are low-field experimental data. Dashed line - Altshuler h/2e contribution; dotted line, assumed h/e contribution. Light solid line, sum of these two terms. h/2e period is ~24G. Inset: high-field h/e oscillations. ℓ_ϕ = 0.9 μm.

One should note first that the effects at 1K are rather small, $\delta R/R \sim 10^{-4}$. Very small measuring voltages must be used to avoid heating these tiny structures. Also, great care must be employed in handling. Otherwise, the wires and rings are easily destroyed by electrical transients.

For the Al rings, Fig. 4a, the AAS oscillations are clearly evident at low fields. Superconducting fluctuations enhance the oscillation amplitude for $T \rightarrow T_c$(= 1.3K). For both the Al and Ag rings, the temperature is such that ℓ_ϕ is less than the ring perimeter; the interference intensity should thus be attenuated compared to Eq. 8. Also, for both rings the low-field (AAS) h/2e oscillations are suppressed by moderate fields (~200G) as expected. Finally, for both samples the sign of the effect is reversed compared to that of Eq. 8. For Al, this is due to superconducting fluctuations. For Ag, this is due to spin-orbit scattering.

For Ag rings, the dominant period at low fields is h/2e (AAS term), but evidence is also seen for an additive h/e contribution at low fields. At higher fields, B > 200G, clear oscillations of period h/e are seen. These persist to the largest field studied, 2 kG. Data from IBM for individual 1 μm rings of linewidth ~40 nm show very clear h/e oscillations at temperatures ~0.1K; these persist up to 160 kG. The IBM studies have also verified the theoretical ideas about the averaging reduction of the h/e oscillations in arrays of N rings with N = 3, 10, or 30. [40]

4. OTHER QUANTUM TRANSPORT PHENOMENA

The effects discussed so far occur in the metallic regime of the MOSFETs and metal wires, where the sample is a "good" conductor and the quantum interference corrections are small. (This regime is usually defined as $k_F \ell \gg 1$.) There are a number of other new quantum effects in this "good-conductor" regime, which we discuss briefly below. These include the mechanisms of inelastic scattering and wavefunction spatial quantization.

4.1 Inelastic/Phase Breaking Times

Central to the picture of electron interference and backscattering is the idea of phase coherence. The electron phase coherence lifetime τ_ϕ is controlled by a number of processes: electron-phonon scattering, electron-electron scattering, and (possibly) electron-defect scattering. It was demonstrated in clean Al films (2D) that the mechanisms determining the rate τ_ϕ^{-1} arise from known processes, and are additive: [4b]

$$\tau_\phi^{-1} = \tau_{e-ph}^{-1} + \tau_{e-e}^{-1} \sim c_3 T^3 + c_1 T \qquad (10)$$

The temperature dependence can be used to identify the mechanisms contributing to the phase-breaking rate. Localization studies of clean metal films and wires ($k_F \ell \gg 1$) and MOSFETs reveal the rates and approximate magnitudes shown in Table III. [4,11,14,41]

Table III Phase-breaking rates (in sec^{-1}); $R_\square$ in ohms, W in μm.

Dimension vs. ℓ_T		Rate	System
2D	τ_{e-ph}^{-1}	$\sim 10^7 T^3$	metal films
	τ_{e-e}^{-1}	$\sim 10^8 R_\square T$	metal films and MOSFETs (low T)
		$\sim T^2$	metal films and MOSFETs (high T)
1D	τ_{e-ph}^{-1}	$\sim 10^7 T^3$	metal films
	τ_{e-e}^{-1}	$\sim 10^8 (R_\square/W)^{2/3} T^{2/3}$	metal wires [11]

The electron-phonon rate in clean metal films and wires is due to 3D electron-phonon scattering in the range of temperatures and film parameters studied to date. This is because the average phonon wavelength is less than the film thickness. In typical Al films, electron-phonon scattering is dominant only above 5K, and λ_{avg} = 75 nm/T < d. Thus, for this temperature range the scattering rate is 3D.

The electron-electron rates do depend on system dimensionality for samples studied to date. This is because the size scale determining the effective dimensionality is the thermal diffusion length, $\ell_T = (\hbar D/k_B T)^{1/2} \sim 0.2$ μm at 1K. For wires of width less than ℓ_T, this rate is one dimensional. [11]

A number of experiments on dirty ($k_F\ell \to 1$) metal films show phase breaking rates which are $\propto T^2$ [1,15]. This temperature dependence is not yet explained in terms of known mechanisms. It is possible that a new electron-impurity inelastic scattering process occurs in very dirty films ($k_F\ell \sim 1$) and films quench condensed onto a cold substrate. More research needs to be done here.

4.2 Wavefunction Spatial Quantization

Another issue which is addressable in narrow MOSFETs, but not yet in metal wires, is the spatial quantization of the electron wavefunction. In MOSFETs the electron surface density is low enough, for $n_s = 10^{12}$ cm^{-2}, that quanitzation of the electron wavefunctions across the width W of the MOS wire may be observed. (At this density, the effective electron-electron spacing is 10 nm.)

The electron energy spectrum at typical surface densities is [10]

$$E = E_o + \frac{\hbar^2}{2m}\left(\frac{\pi p}{W}\right)^2 + \frac{\hbar^2}{2m}\left(\frac{\pi j}{L}\right)^2 \tag{11}$$

with E_o the energy of the lowest-energy quantized state in the triangular potential well normal to the surface, p and j are positive integers, L is the sample length, and $m = 0.19\ m_o$ for the <100> silicon surface. For typical wire lengths and temperatures, the spacing between adjacent j levels is less than the thermal width, $\Delta E \sim kT$. Thus, motion along the length of the MOS wire has an effectively continuous spectrum.

The energy levels corresponding to the different p values are the particle-in-a-box states familiar from single-particle quantum mechanics. The Fermi energy can be adjusted to sit at any specific energy by varying the gate voltage V_G. Thus one should be able to sweep the Fermi level through a given p state. The density of states is divergent when the energy matches $E_o + \hbar^2(\pi p/W)^2/2m$, since the density of states diverges for small j. This divergence will not be seriously broadened by kT smearing, since typical spacings between adjacent p levels are $(E_{p+1}-E_p) \sim 1$ to 10 meV, whereas $kT \sim 0.1$ meV.

Various experiments have sought to identify the density-of-states peaks from measurements of the conductivity as a function of gate voltage. (Here, $V_{DS} \ll V_G$.) The initial studies on single wires [14b, 42] yielded indications of size-quantization effects but no strong confirmation. It became clear, in any case, that the fabrication and materials requirements were very demanding. The linewidth must be very uniform: $\delta W < 10$ nm. Also, the elastic and inelastic lengths must be as long as possible. It is certainly a requirement that $W < \ell_\phi$ to see these quantized states. Otherwise, the electron will lose its phase memory before traversing the width. It appears that it is not necessary for ℓ to exceed W. [14b, 16]

Recent experiments at MIT [16] and Yale [43] provide more convincing evidence for size-quantized electron states. The MIT experiments used a parallel array of 250 inversion layer wires, each ~50 nm wide. The oscillation in the transconductance vs. V_G was interpreted in terms of size-quantized states. The Yale experiments correlated changes in electron specific heat with conductivity oscillations. The specific heat showed much larger changes, as expected. The specific heat can be more directly related to the electron density of states. This is an area deserving further experiment and also theoretical study, especially vis-a-vis possible device implications.

4.3 Conductance Fluctuations due to Fluctuating Trap States

There are also a number of new phenomena observable in the regime where the sample is a **poor** conductor. These include the modulation of the conductance by a single trap state. Systems in which this has been observed are MOSFETs [8,41] where the electron density is controlled with the gate voltage, and small-area tunnel junctions [42]. With a tunnel junction, the conductivity can be varied over orders of magnitude by controlling the thickness of the tunnel oxide. Atomic scale motion of a single defect state, due to electron filling or unfilling, can cause large changes in the conductance, giving rise to "telegraph noise." [41,42] The superposition of this switching noise for a number of traps can give random noise with a 1/f spectral density. [42] As seen in these studies, small electrical distortions can influence significantly the current flow in such devices. Thus, small devices form an exciting new laboratory for studying behavior of individual defect states.

5. CONCLUSIONS AND ACKNOWLEDGEMENTS

The transport studies described in Sec. 3 and 4 demonstrate the striking effects of electron wave interference in the low temperature electron transport properties. Most of these studies would have been impossible without advanced microfabrication techniques. The scientific experiments to date have dealt with electron energies within k_BT (0.1 meV) of E_F, at temperatures of a few Kelvin. Recent studies of new semiconductor device structures, such as the tunneling hot-electron transistor [46], use electron injection energies of several hundred meV above the conduction band edge. The techniques described in this paper have so far dealt with electron distributions very near thermal equilibrium. Application of these techniques in the future to probe inelastic scattering, electron reflection coefficients at interfaces, and phase coherence effects for electrons **far** from equilibrium represents a new and challenging direction for this research. Success in that venture could yield significant scientific and technological benefits.

The author thanks his colleagues at Yale for much instruction and shared excitement in the research described in this paper. These colleagues include P. Santhanam, S. Wind, V. Chandrasekhar, M. Rooks, P. McEuen, R. G. Wheeler, and Y. Imry, who also taught outstanding courses at Yale in this field. Extensive and instructive discussions with R. E. Howard and G. Deutscher, and Fellowship support by the Fulbright Foundation, are also gratefully acknowledged.

REFERENCES

[1] Bergmann, G., Phys Rep. **107** (1984) 1.
[2] **Localization, Interaction and Transport Phenomena**, Kramer, B., Bergmann, G. and Bruynseraede, Y. (eds.) (Springer-Verlag, Berlin, 1985); Dynes, R.C., Physica (Amsterdam) **109** & **110B** (1982) 1857.
[3] Lee, P.A. and Ramakrishnan, T.V., Rev. Mod. Phys. **57** (1985) 287.
[4] a. Santhanam, P., Wind, S. and Prober, D.E., Phys. Rev. Lett. **53** (1984) 1179, and Phys. Rev. B, to be published; b. Santhanam, P. and Prober, D.E., Phys. Rev. B **29** (1984) 3733.
[5] Imry, Y., Physics of Mesoscopic Systems, chapter in **Directions in Condensed Matter Physics, Vol. I** (World Scientific, Singapore, 1986).
[6] Aronov, A.G. and Sharvin, Yu.V., Rev. Mod. Phys., to be published.
[7] Howard, R. E. and Prober, D. E., Nanometer Scale Fabrication Techniques, in **VLSI Electronics: Microstructure Science Vol. V**, Einspruch, N.E. (ed) (Academic Press, New York 1982), p. 145.
[8] Howard, R.E., Skocpol, W.J. and Jackel, L.D., Ann. Rev. Mater. Sci. **16** (1986) 441.

[9] Mackie, S. and Beaumont, S.P., Solid State Technol. **28**, No. 8 (1985) 117.
[10] Ando, T., Fowler, A.B., and Stern, F., Rev. Mod. Phys. **54** (1982) 437.
[11] Wind, S., Rooks, M.J., Chandrasekhar, V. and Prober, D.E., Phys. Rev. Lett. **57** (1986) 633.
[12] Stone, A.D., Phys. Rev. Lett. **54** (1985) 2692.
[13] Skocpol, W.J., et al., Surf. Sci. **170** (1986) 1.
[14] a. Wheeler, R.G. et al., Phys. Rev. Lett. **49** (1982) 1674; b. Wheeler, R.G., Choi, K.K. and Wisnieff, R., Surf. Sci. **142** (1984) 19.
[15] Licini, J.C. et al., Phys. Rev. Lett. **55** (1985) 2987.
[16] Warren, A.C., Antoniadis, D.A. and Smith, H.I., Phys. Rev. Lett. **56** (1986) 1858.
[17] Dean, C.C. and Pepper, M., J. Phys. C **15** (1982) L1287.
[18] Kaplan, S.B. and Harstein, A., Phys. Rev. Lett. **56** (1986) 2403.
[19] Thornton, T. J. et al., Phys. Rev. Lett. **56** (1986) 1198.
[20] Choi, K. K. et al., unpublished, and Bull. Amer. Phys. Soc.**31**(1986) 606.
[21] Flanders, D.C. and White, A.E., J. Vac. Sci. Technol. **19** (1981) 892.
[21a] Prober, D.E., Feuer, M.D. and Giordano, N.,Appl. Phys. Lett.**37**(1980) 94.
[22] Rooks, M.J., Wind, S., McEuen, P.L. and Prober, D.E., J. Vac. Sci. Technol., to be published.
[23] Thouless, D.J., Phys. Rev. Lett. **39** (1977) 1167.
[24] Akkermans, E., Wolf, P.E., and Maynard, R.,Phys. Rev. Lett.**56**(1986) 1471.
[25] Lee, P.A. and Stone, A.D., Phys. Rev. Lett. **55** (1985) 1622.
[26] Al'tshuler, B.L. and Khmel'nitskii, D.E., JETP Lett. **42** (1985) 359.
[27] Skocpol, W.J. et al., Phys. Rev. Lett. **56** (1986) 2865.
[28] Al'tshuler, B.L., Aronov, A.G. and Spivak, B.Z., JETP Lett. **33**(1981) 94.
[29] Stone, A.D. and Imry, Y., Phys. Rev. Lett. **56** (1986) 189.
[30] Sharvin, D. Yu and Sharvin, Yu. V., Pis'ma Zh. Eksp. Teor. Fiz. **34** (1981) 285 [JETP Lett **34** (1981) 272].
[31] Gefen, Y., Imry, Y. and Azbel, M. Ya., Phys. Rev. Lett. **52** (1984) 129.
[32] Buttiker, M. et al., Phys. Rev. B **31** (1985) 6207.
[33] Pannetier, B. et al., Phys. Rev. Lett. **53** (1984) 718.
[34] Dolan, G.J., Licini, J.C. and Bishop, D.J., Phys. Rev.Lett.**56**(1986) 1493.
[35] Claeson, T. et al., **Proc. SQUID 85** (Walter de Gruyter, Berlin, New York).
[36] Webb, R.A. et al., Phys. Rev. Lett. **54** (1985) 2696.
[37] Chandrasekhar, V., Rooks, M.J., Wind, S. and Prober, D.E., Phys. Rev. Lett. **55** (1985) 1610.
[38] Datta, S. et al., Phys. Rev. Lett. **55** (1985) 2344.
[39] Umbach, C.P. et al., Phys. Rev. B **30** (1984) 4048.
[40] Umbach, C.P. et al., Phys. Rev. Lett. **56** (1986) 386.
[41] Uren, M.J., Davies, R.A. and Pepper, M., J. Phys. C**13** (1980) L985.
[42] Skocpol, W.J. et al., Surf. Sci. **170** (1986) 1.
[43] Wisnieff, R.L. and Wheeler, R.G., to be published
[44] Howard, R.E. et al., IEEE Trans. Elect. Devices **ED-32** (1985) 1669.
[45] Rogers, C.T. and Buhrman, R.A., Phys. Rev. Letters **53** (1984) 1272, and Phys. Rev. Letters **55** (1985) 859.
[46] Heiblum, M. et al., Appl. Phys. Lett. **47**, (1985) 1105.